

Interference effects for Higgs-mediated Z -pair plus jet production

John M. Campbell,^{*} R. Keith Ellis,[†] Elisabetta Furlan,[‡] and Raoul Röntsch[§]

Fermilab, PO Box 500, Batavia, IL 60510, USA

(Dated: August 8, 2018)

We study interference effects in the production channel ZZ +jet, in particular focusing on the role of the Higgs boson. This production channel receives contributions both from Higgs boson-mediated diagrams via the decay $H \rightarrow ZZ$ (signal diagrams), as well as from diagrams where the Z -bosons couple directly to a quark loop (background diagrams). We consider the partonic processes $gggZZ$ and $gq\bar{q}ZZ$ in which interference between signal and background diagrams first occurs. Since interference is primarily an off-resonant effect for the Higgs boson, we treat the Z -bosons as on-shell. Thus our analysis is limited to the region above threshold, where the invariant mass of the Z -pair, m_{ZZ} , satisfies the condition $m_{ZZ} > 2m_Z$. In the region $m_{ZZ} > 300$ GeV we find that the interference in the ZZ + jet channel is qualitatively similar to interference in the inclusive ZZ channel. Moreover, the rates are sufficient to study these effects at the LHC once jet-binned data become available.

1. INTRODUCTION

The discovery of a Higgs boson at the Large Hadron Collider (LHC) with a mass of around 125 GeV [1, 2] obliges us to undertake a program of precision measurements that will take more than a decade to complete. Since the observed particle, by virtue of its spin and the pattern of its couplings, is quite different than any other particle observed to date, it will be important to examine *all* the features of this particle. Kauer and Passarino made the interesting observation [3] that the narrow width approximation is inadequate to describe the spectrum of the Higgs decay products in the channels $H \rightarrow VV$ (where V is a vector boson). In fact a sizeable fraction $\sim 10\%$ of the Higgs-mediated cross section lies in a high mass tail, where the mass of the decay products is greater than $2m_V$. The unique feature of this tail is that it is dependent on the couplings of the Higgs, both in production and decay, but, unlike measurements made on the Higgs boson peak, it is independent of the Higgs boson width. Subsequently a number of proposals have been made to exploit this high mass tail, either to bound the width of the Higgs boson [4–6] or to investigate the nature of the gluon-Higgs coupling [7, 8]. Recent measurements by both the ATLAS [9] and CMS [10] collaborations using this feature place bounds on the Higgs width at the level of $\Gamma_H/\Gamma_H^{\text{SM}} \simeq 5 - 10$. These bounds rely on the assumption that the Higgs couplings as measured off-shell agree with the Higgs couplings on-shell. It is possible to construct models where this is not the case [11]. Independent of such measurements, however, an understanding of the off-shell behavior of the Higgs boson is important in its own right and will be pursued vigorously once data-taking resumes at the LHC next year.

In this paper we consider $H \rightarrow ZZ$ decays, although we expect qualitatively similar effects in the $H \rightarrow W^+W^-$ channel. The extraction of the Higgs contribution $gg \rightarrow H \rightarrow ZZ \rightarrow 4l$ in the high mass tail is challenging because the rate is an order of magnitude smaller than the $pp \rightarrow ZZ \rightarrow 4l$ background, as shown in Fig. 1. Since the gluon-gluon initial state responsible for Higgs boson

^{*}Electronic address: johnmc@fnal.gov

[†]Electronic address: ellis@fnal.gov

[‡]Electronic address: efurlan@fnal.gov

[§]Electronic address: rontsch@fnal.gov

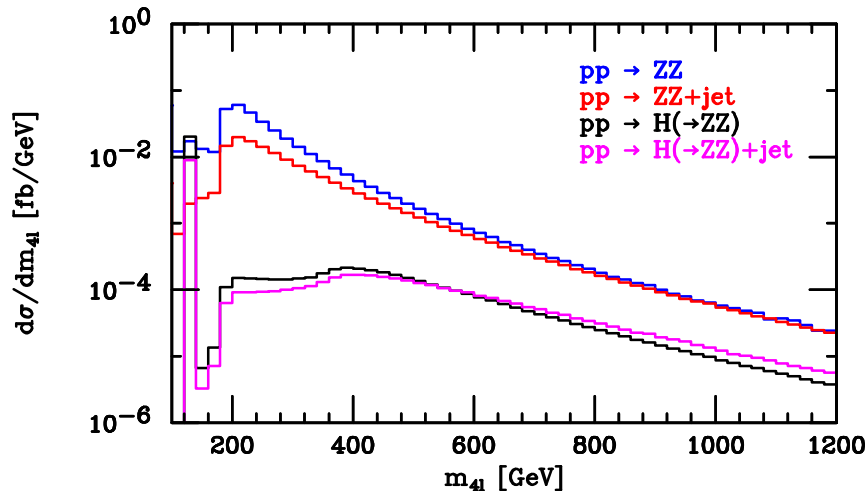


FIG. 1: Zero- and one-jet gluon fusion Higgs production with $H \rightarrow ZZ \rightarrow 4l$ decay as a function of the four-lepton invariant mass m_{4l} (lower two curves), together with the leading order backgrounds $pp \rightarrow ZZ \rightarrow 4l$ and $pp \rightarrow ZZ(\rightarrow 4l) + \text{jet}$ (upper two curves). The results are for the LHC at $\sqrt{s} = 8$ TeV, and a jet cut of $p_T > 30$ GeV. The Z -bosons are taken to decay leptonically, with a cut $m_{ll} > 20$ GeV imposed on their decay products. All results are produced using MCFM [23].

production radiates copiously, the cross section for a Higgs boson produced in association with a jet is expected to be large [12]. Indeed, as can be seen in Fig. 1, the production cross section for an off-shell Higgs with four-lepton invariant mass $m_{4l} > 300$ GeV in the exclusive one-jet bin is comparable to that in the zero-jet bin, for a typical jet cut $p_{T,j} > 30$ GeV. On the other hand, for $m_{4l} > 300$ GeV, the cross section for the leading order (LO) exclusive $pp \rightarrow ZZ + \text{jet}$ production is a factor of 1.5 smaller than that for inclusive $pp \rightarrow ZZ$. It is thus clear that in the tail, the ratio of Higgs signal to leading order background is better in the one-jet bin than in the zero-jet bin. An examination of the gluon-Higgs coupling, or a constraint on the Higgs width, from the one-jet bin can therefore be competitive with one from the zero-jet bin. So far the ATLAS collaboration has provided jet-binned differential distributions of the Higgs boson only in the $\gamma\gamma$ channel [13]. In due course data will also become available in the ZZ channel. Anticipating this development, in this paper we will study off-resonant Higgs boson effects in the $ZZ + \text{jet}$ channel.

For a calculation extending into the high mass tail, the dependence on the top mass must be retained. The leading-order amplitudes contain one loop, and have been calculated in Ref. [12]. The next-to-leading order (NLO) corrections, which involve two-loop amplitudes, are very challenging and have not yet been calculated. Note that, in the case where the heavy top limit is applicable, the relevant amplitudes have been known to NLO for some time [14–17], and next-to-next-to-leading order (NNLO) results in the dominant gg channel have been calculated recently [18, 19].

From the outset it was clear that an accurate description of the high mass region requires that interference with non-Higgs mediated diagrams be taken into account [3, 20–22]. Indeed, the main role of the Higgs boson is to cancel the bad high-energy behavior that results from the presence of longitudinal polarizations of W - and Z -bosons. Thus the existence of this cancellation guarantees that interference will be important in the high mass region. We must therefore also calculate non-Higgs mediated $ZZ + \text{jet}$ production through a quark loop.

The relevant parton processes for the production of a pair of Z -bosons in association with a jet are given in Table I and representative Feynman diagrams are shown in Figs. 2 and 3. The lowest order at which this occurs is through the partonic reaction

$$\mathcal{B}_1^{(c)} : q + \bar{q} \rightarrow ZZ + g, \quad (1)$$

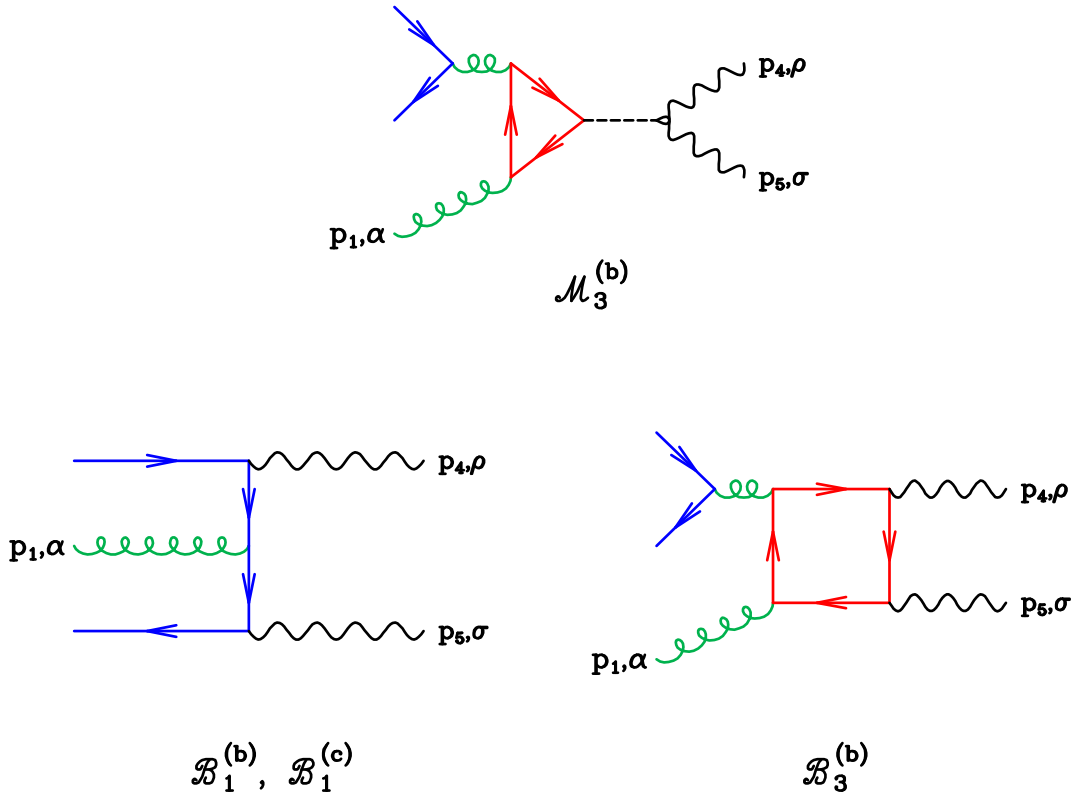


FIG. 2: Representative diagrams for the $0 \rightarrow gq\bar{q}ZZ$ amplitude.

where the subscript indicates the order in the strong coupling, g_s , at which the amplitude first occurs. At the level of the matrix element squared, process (1) enters at order $g_s^2 g_W^4$. The superscript is used to differentiate between partonic channels that enter at the same order. For instance there are also the crossed processes with a gluon in the initial state, such as,

$$\mathcal{B}_1^{(b)} : q + g \rightarrow ZZ + q . \quad (2)$$

The NLO corrections to the processes (1) and (2), including all crossings, have been presented in Refs. [24–26]. In addition, ingredients for the NLO ZZ +jet process are part of the NNLO ZZ

Amplitude name	Process	Order of Amplitude
$\mathcal{M}_3^{(a)}$	$g + g \rightarrow H(\rightarrow ZZ) + g$	$g_s^3 g_W^2$
$\mathcal{B}_3^{(a)}$	$g + g \rightarrow ZZ + g$	$g_s^3 g_W^2$
$\mathcal{M}_3^{(b)}$	$q + g \rightarrow H(\rightarrow ZZ) + q$	$g_s^3 g_W^2$
$\mathcal{B}_1^{(b)}$	$q + g \rightarrow ZZ + q$	$g_s g_W^2$
$\mathcal{B}_3^{(b)}$	$q + g \rightarrow ZZ + q$	$g_s^3 g_W^2$
$\mathcal{B}_1^{(c)}$	$q + \bar{q} \rightarrow ZZ + g$	$g_s g_W^2$

TABLE I: Selection of parton processes for the ZZ + jet process. Representative diagrams are shown in Figs. 2 and 3.

calculation presented in Ref. [27]. Merging to a parton shower generator has been considered in Ref. [28].

Focusing on the one-loop corrections to the process (2), we find two classes of contributions that are separately gauge invariant and finite. One represents box diagrams where the Z -bosons are radiated from a closed loop of fermions,

$$\mathcal{B}_3^{(b)} : q + g \xrightarrow{box} ZZ + q . \quad (3)$$

and the other corresponds to diagrams in which a Higgs boson is produced through a massive quark loop and subsequently decays to a pair of Z -bosons,

$$\mathcal{M}_3^{(b)} : q + g \rightarrow H(\rightarrow ZZ) + q . \quad (4)$$

The background process $\mathcal{B}_3^{(b)}$ proceeds by a loop of quarks of all flavors, while $\mathcal{M}_3^{(b)}$ receives significant contributions only for t and b quarks circulating in the loop. Both processes (3) and (4) interfere with the process (2), giving contributions of order $g_s^4 g_W^4$. However, the interference of (2) and (3) is known to be small [24]. Similarly, the interference between (2) and the Higgs-mediated process (4) is also small in the inclusive case [4], as expected by unitarity. We will verify in this paper that this hierarchy holds in the one-jet exclusive bin as well. Partonic crossings of processes (3) and (4) give rise to processes $q + \bar{q} \xrightarrow{box} ZZ + g$ and $q + \bar{q} \rightarrow H(\rightarrow ZZ) + g$ which

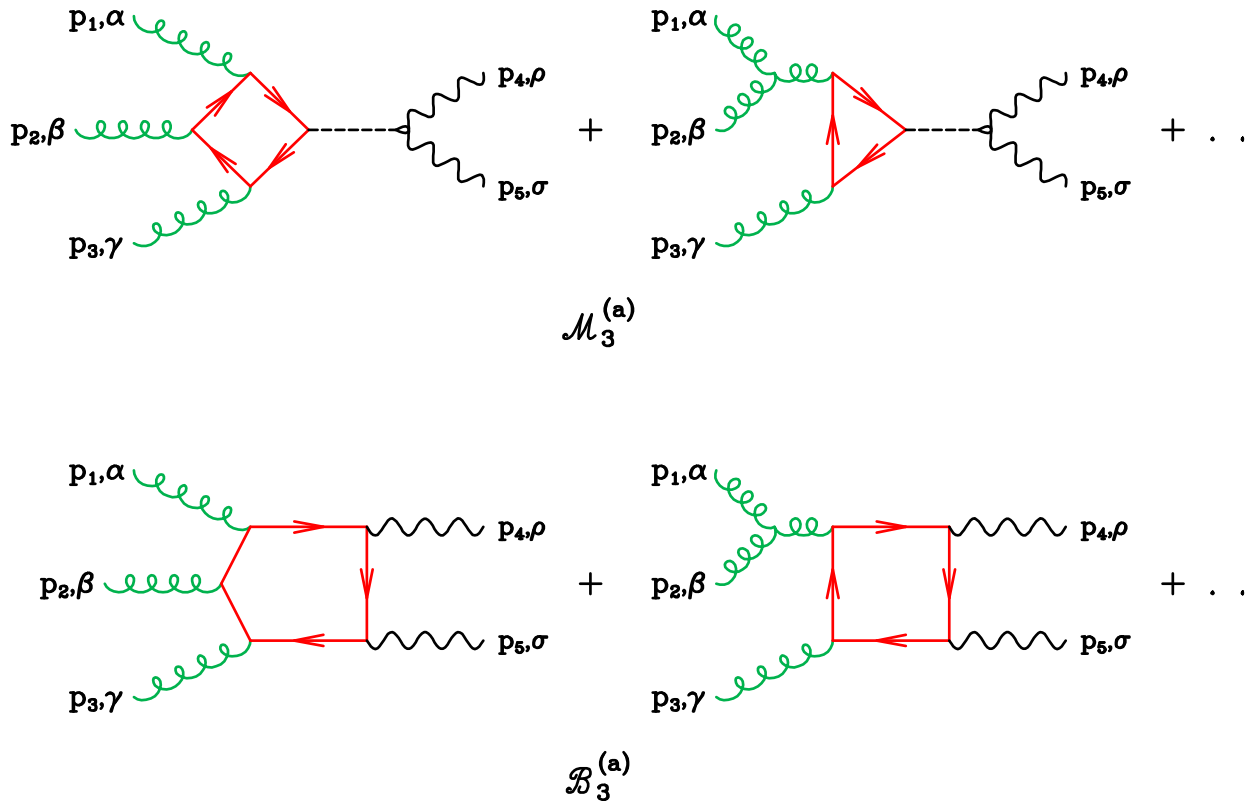


FIG. 3: Representative diagrams for the $0 \rightarrow gggZZ$ amplitude.

interfere with process (1). However, these amplitudes can be trivially obtained from processes (3) and (4), so there is no need to consider them separately.

At the next order, $g_s^6 g_W^4$, the squared loop amplitudes for production of a Z -pair in association with a jet enter. As well as the square of the gg processes (3) and (4) and their interference, gluon-induced production is also present at this order, either through Higgs production

$$\mathcal{M}_3^{(a)} : g + g \rightarrow H(\rightarrow ZZ) + g , \quad (5)$$

or through loops of quarks in a similar fashion to the process (3),

$$\mathcal{B}_3^{(a)} : g + g \rightarrow ZZ + g . \quad (6)$$

The gluon-induced process $\mathcal{B}_3^{(a)}$ is known to provide contributions to $VV + \text{jet}$ production in the range of 5-10% [28–30]. Since these represent a NNLO correction to the continuum $pp \rightarrow ZZ + \text{jet}$ process we do not consider them in this work. Likewise, we do not consider the square of $\mathcal{B}_3^{(b)}$. Instead, we confine our studies to the Higgs processes, i.e. the squares of processes (4) and (5), and interference between processes (3) and (4), and between processes (5) and (6). The latter interference has been shown to lead to strong destructive interference in the high mass tail [22]. Indeed, the results of Ref. [22] demonstrate the viability of studying interference effects in the Higgs + jet channel. In this paper, we extend the analysis to include the interference of processes (3) and (4), which contributes at the level of 25-40%, depending on the transverse momentum cut on the jet.

In addition to their use in studying interference effects in Higgs + jet production, the above contributions are necessary to extend the analysis of Ref. [4, 6] to NLO. This is especially important given the slow perturbative convergence of the Higgs cross sections and the corresponding large scale uncertainties and k -factors [31, 32]. In particular, the amplitudes of processes (3)-(6) make up the real radiation corrections to $gg \rightarrow ZZ$ and $gg \rightarrow H(\rightarrow ZZ)$. For this reason, we obtain analytic formulae for the contributions arising from the amplitudes (3)-(6), although the formulae are too long to present in this paper. This will allow a numerically stable computation of these amplitudes that can be integrated over the singular regions. This issue requires particular care because the real radiation amplitudes are at one-loop, rather than the tree-level amplitudes found in conventional NLO calculations.

The virtual contribution for the NLO calculation consists of two-loop amplitudes, including the two loop $gg \rightarrow ZZ$ process. This is an extremely challenging calculation, which may be simplified if one limits the scales involved to s, t, m_q and m_Z , where s, t are the usual Mandelstam variables and m_q is the mass of the quark circulating in the loop. We therefore consider both Z -bosons to be on their mass shells and sum over their polarizations in this work, with a view to extending the calculation of gluon-induced inclusive ZZ production to NLO. Thus our calculation will be appropriate for the region where the invariant mass of the Z -boson pair, $m_{ZZ} > 2m_Z$. As justification for this approximation, we can compare the calculation of $gg \rightarrow Z^{(*)}Z^{(*)}$ from Ref. [4] with a simplified calculation where both Z -bosons are on their mass shells. The results of this comparison are shown in Fig. 4. Although there are differences between the calculations in the ZZ threshold region, for $m_{4l} > 300$ GeV the two are essentially indistinguishable.

2. LOOP AMPLITUDES FOR ZZ PRODUCTION

Although our principal focus will be the production of a pair of vector bosons in association with a jet, we will first consider the process without a jet, which will serve to set up the notation. Representative Feynman diagrams for this process are shown in Fig. 5. By analogy with

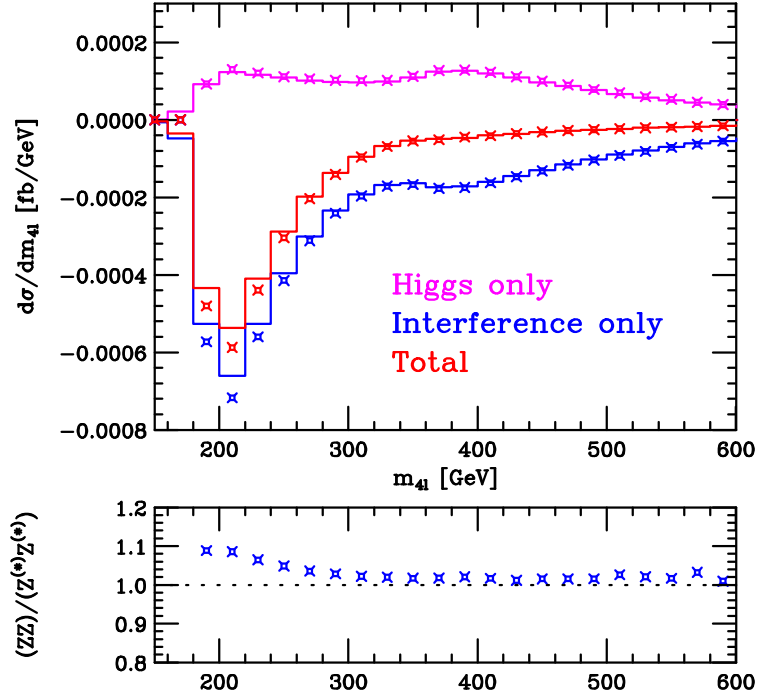


FIG. 4: Difference between the calculation of $gg \rightarrow Z^{(*)}Z^{(*)}$ (histograms), and $gg \rightarrow ZZ$ where both Z -bosons are on their mass shells (points). The lower pane shows the ratio for the interference terms.

Name	Process	Order of Amplitude
$\mathcal{M}_2^{(a)}$	$g + g \rightarrow H(\rightarrow ZZ)$	$g_s^2 g_W^2$
$\mathcal{B}_2^{(a)}$	$g + g \rightarrow ZZ$	$g_s^2 g_W^2$

TABLE II: Selection of parton processes for the ZZ process. Representative diagrams are shown in Fig. 5.

processes (5) and (6), we will refer to the amplitude for the Higgs signal process as $\mathcal{M}_2^{(a)}$ and that for the continuum background as $\mathcal{B}_2^{(a)}$, see Table II. These amplitudes were first studied for on-shell Z -bosons in Ref. [20]; more recently, the Z decay and off-shell effects were also calculated [4]. In our results, we keep the Z -bosons on-shell and sum over the polarizations.

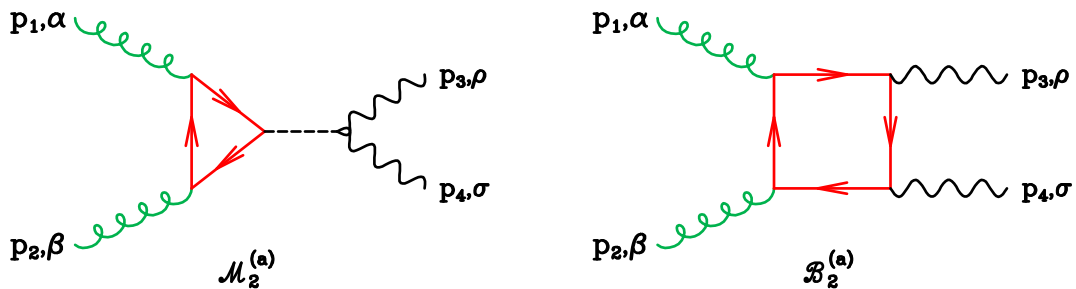


FIG. 5: Representative diagrams for the $0 \rightarrow ggZZ$ amplitude.

$D_{\{1,3,2\}}$	$D_0(p_1, p_3, p_2; m, m, m, m)$	$C_{\{1,2\}}$	$C_0(p_1, p_2; m, m, m)$
$D_{\{2,1,3\}}$	$D_0(p_2, p_1, p_3; m, m, m, m)$	$C_{\{12,3\}}$	$C_0(p_{12}, p_3; m, m, m)$
$D_{\{1,2,3\}}$	$D_0(p_1, p_2, p_3; m, m, m, m)$	$C_{\{1,3\}}$	$C_0(p_1, p_3; m, m, m)$
$B_{\{23\}}$	$B_0(p_{23}; m, m)$	$C_{\{2,3\}}$	$C_0(p_2, p_3; m, m, m)$
$B_{\{123\}}$	$B_0(p_{123}; m, m)$	$C_{\{1,23\}}$	$C_0(p_1, p_{23}; m, m, m)$

TABLE III: Definitions of the scalar integrals that appear in this paper. The notation for the scalar integrals follows Ref. [35].

2.1. Amplitude for $gg \rightarrow H \rightarrow ZZ$

We begin by looking at the amplitude for Higgs production, corresponding to the left hand side of Fig. 5(a), with all momenta outgoing. The resultant amplitude is

$$\mathcal{M}_2^{(a),\alpha\beta} = -i \frac{g_W}{4m_W} \frac{g_s^2}{16\pi^2} \frac{1}{2} \delta_{AB} \overline{M}(s_H) \left(g^{\alpha\beta} - \frac{p_2^\alpha p_1^\beta}{p_1 \cdot p_2} \right) \quad (7)$$

where A, B are the color indices, $g_W = e/\sin\theta_W$ and e, m_W, θ_W are the electric charge, W -boson mass, and the Weinberg angle and $s_H = p_H^2 \equiv 2p_1 \cdot p_2$. Our conventions for the Feynman rules are as given in Ref. [33]. From Ref. [34], the loop function for this amplitude is

$$\overline{M}(s_H) = 8m_q^2 \left[2 - (s_H - 4m_q^2) C_{\{1,2\}} \right], \quad (8)$$

where m_q is the mass of the quark circulating in the loop. $C_{\{1,2\}}$ is a scalar triangle integral; the exact definition is given in Table III and Appendix A. In the limit $m_q \rightarrow \infty$ we have that $\overline{M}(s_H) \rightarrow \frac{8}{3}s_H$.

For the calculation at hand we also need the decay amplitude, depicted on the right hand side of Fig. 5(a). This amplitude is given by,

$$\mathcal{M}^{\rho\sigma}(H \rightarrow ZZ) = ig_W \frac{m_W}{\cos^2\theta_W} g^{\rho\sigma}. \quad (9)$$

Hence, combining Eqs. (7,9) the full amplitude for production and decay is

$$\mathcal{M}_2^{(a),\alpha\beta\rho\sigma} = \mathcal{N} \delta_{AB} \overline{M}(s_H) \frac{1}{s_H - M_H^2} \left(g^{\alpha\beta} - \frac{p_2^\alpha p_1^\beta}{p_1 \cdot p_2} \right) g^{\rho\sigma}, \quad (10)$$

where we have defined an overall normalization factor,

$$\mathcal{N} = i \frac{g_W^2}{4 \cos^2\theta_W} \frac{g_s^2}{16\pi^2} \frac{1}{2}. \quad (11)$$

From this it is straightforward to square the amplitude to obtain the result for the Higgs diagrams alone. The sum over the polarizations of the gluons and the Z -bosons of momentum p can be performed as usual with the projection operators,

$$P_g^{\mu\nu} = -g^{\mu\nu}, \quad P_Z^{\rho\beta}(p) = -g^{\rho\beta} + \frac{p^\rho p^\beta}{m_Z^2}. \quad (12)$$

Including also the sum over colors yields the matrix element squared for the signal in this channel,

$$\mathcal{S}_{gg} \equiv \mathcal{M}_2^{(a),\alpha\beta\rho'\sigma'} (\mathcal{M}_{2,\alpha\beta\rho\sigma}^{(a)})^* P_{Z\rho'}^\rho(p_3) P_{Z\sigma'}^\sigma(p_4) = |\mathcal{N}|^2 \frac{V}{2} \frac{|\overline{M}(s_H)|^2}{(s_H - M_H^2)^2} \left[8 + \left(\frac{s_H - 2m_Z^2}{m_Z^2} \right)^2 \right], \quad (13)$$

where we use the notation for the color factor $V = N_c^2 - 1 = 8$.

2.2. Coupling structure for $gg \rightarrow ZZ$

We turn now to the amplitude shown in Fig. 5(b). We are not interested in the square of this amplitude, which is an NNLO contribution to the continuum $pp \rightarrow ZZ$ production. Rather, our focus is on the interference with the Higgs-mediated amplitude presented in the previous section. We shall consider a single quark of flavor f to be circulating in the quark loop. The Standard Model coupling of this fermion to a Z -boson is given by,

$$-i \frac{g_W}{2 \cos \theta_W} \gamma^\mu (v_f - a_f \gamma_5), \quad v_f = \tau_f - 2Q_f \sin^2 \theta_W, \quad a_f = \tau_f, \quad \tau_f = \pm \frac{1}{2}. \quad (14)$$

The amplitude can be written by extracting an overall factor, given in Eq. (11),

$$\mathcal{B}_2^{(a),\alpha\beta\rho\sigma} = \mathcal{N} \delta_{AB} \left[v_f^2 B_{2,VV}^{(a),\alpha\beta\rho\sigma} + a_f^2 B_{2,AA}^{(a),\alpha\beta\rho\sigma} + v_f a_f \left(B_{2,AV}^{(a),\alpha\beta\rho\sigma} + B_{2,VA}^{(a),\alpha\beta\rho\sigma} \right) \right], \quad (15)$$

where the V and A subscripts indicate the vector and axial vector coupling to the Z -bosons, respectively. The cross-terms proportional to $v_f a_f$ vanish, so that we can write

$$\mathcal{B}_2^{(a),\alpha\beta\rho\sigma} = \mathcal{N} \delta_{AB} \left[(v_f^2 + a_f^2) B_{2,VV}^{(a),\alpha\beta\rho\sigma} + a_f^2 \left(B_{2,AA}^{(a),\alpha\beta\rho\sigma} - B_{2,VV}^{(a),\alpha\beta\rho\sigma} \right) \right]. \quad (16)$$

This decomposition of the coupling structure is particularly useful since the combination of amplitudes $B_{2,AA} - B_{2,VV}$ vanishes in the limit $m_q \rightarrow 0$.

2.3. Projection of interference for $gg \rightarrow ZZ$

With the amplitudes outlined above it is straightforward to compute the interference. The relevant combination is,

$$\mathcal{I}_{gg} \equiv 2 \left(\mathcal{M}_{2,\alpha\beta\rho'\sigma'}^{(a)} \right)^* \mathcal{B}_2^{(a),\alpha\beta\rho\sigma} P_{Z\rho}^{\rho'}(p_3) P_{Z\sigma}^{\sigma'}(p_4) \quad (17)$$

$$\begin{aligned} &= 2V |\mathcal{N}|^2 \overline{M}(s_H)^* \frac{1}{s_H - M_H^2} \left(g_{\alpha\beta} - \frac{p_{2\alpha} p_{1\beta}}{p_1 \cdot p_2} \right) \times \\ &\quad \left[(v_f^2 + a_f^2) B_{2,VV}^{(a),\alpha\beta\rho\sigma} + a_f^2 \left(B_{2,AA}^{(a),\alpha\beta\rho\sigma} - B_{2,VV}^{(a),\alpha\beta\rho\sigma} \right) \right] P_{Z\rho}^{\rho'}(p_3) P_{Z\sigma\rho'}(p_4) \\ &= 2V |\mathcal{N}|^2 \frac{2 \overline{M}(s_H)^*}{s_H - M_H^2} \left[(v_f^2 + a_f^2) I_{VV} + a_f^2 I_{(AA-VV)} \right], \end{aligned} \quad (18)$$

where the projections are given by,

$$\begin{aligned}
I_{VV} = & 32 \left(m_q^2 (2p_1 \cdot p_2 - m_Z^2 - 2m_q^2) (D_{\{1,2,3\}} + D_{\{2,1,3\}}) \right. \\
& + \left(1 - \frac{m_Z^2 + 2m_q^2}{p_1 \cdot p_2} \right) \left((p_2 \cdot p_3 p_1 \cdot p_3 + p_1 \cdot p_2 m_q^2 - \frac{1}{2} p_1 \cdot p_2 m_Z^2) D_{\{1,3,2\}} \right. \\
& \left. \left. - p_1 \cdot p_3 C_{\{1,3\}} - p_2 \cdot p_3 C_{\{2,3\}} \right) + 2m_q^2 C_{\{1,2\}} + 1 \right) \quad (19)
\end{aligned}$$

$$\begin{aligned}
I_{(AA-VV)} = & 64m_q^2 \left((D_{\{1,3,2\}} + D_{\{2,1,3\}} + D_{\{1,2,3\}}) \frac{m_q^2}{m_Z^4} (3m_Z^4 - 2p_1 \cdot p_2 m_Z^2 + p_1 \cdot p_2^2) \right. \\
& - \frac{(p_1 \cdot p_2 - 3m_Z^2)}{m_Z^2 p_1 \cdot p_2} \left[\frac{1}{2} (2p_2 \cdot p_3 p_1 \cdot p_3 - p_1 \cdot p_2 m_Z^2) D_{\{1,3,2\}} - p_1 \cdot p_3 C_{\{1,3\}} - p_2 \cdot p_3 C_{\{2,3\}} \right] \\
& \left. - p_1 \cdot p_2 (D_{\{1,2,3\}} + D_{\{2,1,3\}}) + C_{\{1,2\}} \frac{p_1 \cdot p_2}{m_Z^4} (p_1 \cdot p_2 - m_Z^2) \right). \quad (20)
\end{aligned}$$

The notation for the scalar integrals D and C is given in Table III. We note that, in contrast to the case where the Z -bosons are off-shell and their decays included, these formulae for the interference take a very simple form. In particular, there are no denominators of the form $1/p_T^2$, where p_T is the transverse momentum of one of the Z -bosons.

3. AMPLITUDES FOR $ZZ + \text{jet}$ PRODUCTION

We turn now to the amplitudes for $ZZ + \text{jet}$ production. The partonic amplitudes are given in Eqs. (2-6) and Table I and are depicted in Figs. 2 and 3. The large-energy behavior of the background loop amplitudes $\mathcal{B}_3^{(a)}$ and $\mathcal{B}_3^{(b)}$ is unitarized by the Higgs amplitudes $\mathcal{M}_3^{(a)}$ and $\mathcal{M}_3^{(b)}$ respectively. In contrast, the amplitude $\mathcal{B}_1^{(b)}$ is insensitive to the unitarizing effects of the Higgs boson.

3.1. Amplitude for $gq \rightarrow H(\rightarrow ZZ)q$

We begin by looking at the Higgs-mediated process (4). This was first computed in Ref. [12] for an on-shell Higgs. Modifying this result slightly to allow the Higgs to be off-shell, the amplitude is

$$\mathcal{M}_3^{(b),\alpha} = -i \frac{g_s^2}{16\pi^2} \frac{g_W}{4m_W} \frac{1}{2} (t^A)_{32} g_s \frac{1}{s_{23}} \bar{u}(p_3) \gamma_\mu u(p_2) \left(g^{\alpha\mu} - \frac{p_1^\mu (p_2^\alpha + p_3^\alpha)}{p_1 \cdot (p_2 + p_3)} \right) F(s_{23}, s_H) \quad (21)$$

where the loop function $F(s_{23}, s_H)$ is given by

$$F(s_{23}, s_H) = -8m_q^2 \left[2 - (s_H - s_{23} - 4m_q^2) C_{\{1,23\}} + \frac{2s_{23}}{s_H - s_{23}} (B_{\{123\}} - B_{\{23\}}) \right], \quad (22)$$

in terms of the scalar integrals defined in Table III. Note that the loop function above is related to the $gg \rightarrow H$ loop function $\overline{M}(s_H)$ given in Eq. (8) by

$$F(0, s_H) = -\overline{M}(s_H). \quad (23)$$

Including the decay $H \rightarrow Z(p_4)Z(p_5)$, the amplitude is

$$\mathcal{M}_3^{(b),\alpha\rho\sigma} = \mathcal{N} \left(g_s (t^A)_{32} \frac{F(s_{23}, s_H)}{s_H - M_H^2} \right) \frac{1}{s_{23}} \bar{u}(p_3) \gamma_\mu u(p_2) \left(g^{\alpha\mu} - \frac{p_1^\mu (p_2^\alpha + p_3^\alpha)}{p_1 \cdot (p_2 + p_3)} \right) g^{\rho\sigma}, \quad (24)$$

and squaring this we find

$$\begin{aligned} \mathcal{S}_{gq\bar{q}} &\equiv -\mathcal{M}_3^{(b),\alpha\rho\sigma} \left(\mathcal{M}_{3;\alpha\rho'\sigma'}^{(b)} \right)^* P_{Z\rho}^{\rho'}(k_4) P_{Z\sigma}^{\sigma'}(k_5) \\ &= \frac{V}{2} g_s^2 |\mathcal{N}|^2 \frac{1}{s_{23}} \frac{(p_1 \cdot p_2^2 + p_1 \cdot p_3^2)}{p_1 \cdot p_{23}^2} \frac{|F(s_{23}, s_H)|^2}{(s_H - M_H^2)^2} \left[8 + \left(\frac{s_H - 2m_Z^2}{m_Z^2} \right)^2 \right]. \end{aligned} \quad (25)$$

The negative sign in the first line comes from the sum over the gluon polarizations. Recall that \mathcal{N} is our canonical overall factor given in Eq. (11).

3.2. Amplitude for tree-level $qg \rightarrow ZZq$

The tree-level background amplitude in process (2) is given by

$$\begin{aligned} \mathcal{B}_1^{(b),\alpha\rho\sigma} &= \frac{ig_s g_W^2}{4 \cos^2 \theta_W} (t_A)_{32} \bar{u}(p_3) \left((v_f^2 + a_f^2) + 2v_f a_f \gamma_5 \right) \times \\ &\quad \left(T^{\alpha\rho\sigma}(p_1, p_2, p_3, p_4, p_5) + T^{\alpha\sigma\rho}(p_1, p_2, p_3, p_5, p_4) \right) v(p_2), \end{aligned} \quad (26)$$

where the gamma-matrix structure is contained in the function $T^{\alpha\rho\sigma}$:

$$T^{\alpha\rho\sigma}(p_1, p_2, p_3, p_4, p_5) = \frac{\gamma^\alpha \hat{p}_{13} \gamma^\rho \hat{p}_{25} \gamma^\sigma}{s_{13} s_{25}} + \frac{\gamma^\rho \hat{p}_{34} \gamma^\sigma \hat{p}_{12} \gamma^\alpha}{s_{12} s_{34}} + \frac{\gamma^\rho \hat{p}_{34} \gamma^\alpha \hat{p}_{25} \gamma^\sigma}{s_{34} s_{25}}. \quad (27)$$

This amplitude squared is the leading-order contribution to $pp \rightarrow ZZj$. Its interference with the Higgs-mediated amplitude, Eq. (24) is

$$\mathcal{I}_{gq\bar{q}}^{(4)} = -2\mathcal{M}_3^{(b),\mu\rho\sigma} \left(\mathcal{B}_{1,\mu\rho'\sigma'}^{(b)} \right)^* P_{Z\rho}^{\rho'}(k_4) P_{Z\sigma}^{\sigma'}(k_5) \quad (28)$$

where the superscript indicates that the interference is at order g_s^4 .

3.3. Projection of interference for $qg \rightarrow ZZq$

The amplitude of process (3) has the same weak coupling structure as $qg \rightarrow ZZ$, and can therefore be written in terms of vector and axial couplings as in Eq. (16),

$$\mathcal{B}_3^{(b),\alpha\rho\sigma} = \mathcal{N} g_s (t_A)_{32} \bar{u}(p_3) \gamma_\nu u(p_2) \left[(v_f^2 + a_f^2) B_{3,VV}^{(b),\nu\alpha\rho\sigma} + a_f^2 \left(B_{3,AA}^{(b),\nu\alpha\rho\sigma} - B_{3,VV}^{(b),\nu\alpha\rho\sigma} \right) \right], \quad (29)$$

where $B_{3,VV}^{(b)}$ and $B_{3,AA}^{(b)}$ are loop functions. Again, our focus is not on the square of this amplitude but on its interference with the Higgs-mediated process presented in Sec. 3.1. This is given by

$$\begin{aligned} \mathcal{I}_{gq\bar{q}}^{(6)} &\equiv -2\mathcal{M}_{3,\alpha\rho'\sigma'}^{(b)} \left(\mathcal{B}_3^{(b),\alpha\rho\sigma} \right)^* P_{Z\rho}^{\rho'}(k_4) P_{Z\sigma}^{\sigma'}(k_5) \\ &= -2|\mathcal{N}|^2 g_s^2 C_F N_C \frac{F(s_{23}, s_H)}{s_H - M_H^2} \frac{1}{s_{23}} \text{Tr}[\hat{p}_3 \gamma^\mu \hat{p}_2 \gamma_\nu] \left(g_{\alpha\mu} - \frac{p_{1\mu} (p_{2\alpha} + p_{3\alpha})}{p_1 \cdot (p_2 + p_3)} \right) \\ &\quad \times P_{Z\rho}^{\rho'}(k_4) P_{Z\sigma}^{\sigma'}(k_5) \left[(v_f^2 + a_f^2) B_{3,VV}^{\nu\alpha\rho\sigma} + a_f^2 \left(B_{3,AA}^{(a),\nu\alpha\rho\sigma} - B_{3,VV}^{(a),\nu\alpha\rho\sigma} \right) \right]. \end{aligned} \quad (30)$$

3.4. Amplitude for $gg \rightarrow H(\rightarrow ZZ)g$

We now move on to the Higgs and interference contributions through gluon-fusion. The Higgs-mediated contribution, represented by the diagrams in Fig. 3(a), is also presented in Ref. [12]. By combining this with the decay amplitude given in Eq. (9), we obtain the full amplitude for the process at hand,

$$\begin{aligned} \mathcal{M}_3^{(a),\alpha\beta\gamma\rho\sigma} &= -4\mathcal{N}g_s g^{\rho\sigma} \frac{s_H^2}{s_H - M_H^2} f_{ABC} \left[F_2^{\alpha\beta\gamma}(p_1, p_2, p_3) A_3(p_1, p_2, p_3) \right. \\ &+ \left. F_1^{\alpha\beta\gamma}(p_1, p_2, p_3) A_2(p_1, p_2, p_3) + F_1^{\beta\gamma\alpha}(p_2, p_3, p_1) A_2(p_2, p_3, p_1) + F_1^{\gamma\alpha\beta}(p_3, p_1, p_2) A_2(p_3, p_1, p_2) \right]. \end{aligned} \quad (31)$$

The projectors F_1 and F_2 are defined by,

$$\begin{aligned} F_1^{\alpha\beta\gamma}(p_1, p_2, p_3) &= \left(\frac{g^{\alpha\beta}}{p_1 \cdot p_2} - \frac{p_1^\beta p_2^\alpha}{p_1 \cdot p_2^2} \right) \left(\frac{p_2^\gamma}{p_2 \cdot p_3} - \frac{p_1^\gamma}{p_1 \cdot p_3} \right) \\ F_2^{\alpha\beta\gamma}(p_1, p_2, p_3) &= \frac{p_3^\alpha p_1^\beta p_2^\gamma - p_2^\alpha p_3^\beta p_1^\gamma}{p_1 \cdot p_2 p_1 \cdot p_3 p_2 \cdot p_3} + \frac{g^{\alpha\beta}}{p_1 \cdot p_2} \left(\frac{p_1^\gamma}{p_3 \cdot p_1} - \frac{p_2^\gamma}{p_3 \cdot p_2} \right) \\ &+ \frac{g^{\beta\gamma}}{p_2 \cdot p_3} \left(\frac{p_2^\alpha}{p_1 \cdot p_2} - \frac{p_3^\alpha}{p_1 \cdot p_3} \right) + \frac{g^{\alpha\gamma}}{p_1 \cdot p_3} \left(\frac{p_3^\beta}{p_2 \cdot p_3} - \frac{p_1^\beta}{p_2 \cdot p_1} \right) \end{aligned} \quad (32)$$

and the functions A_2 and A_3 contain the loop integral functions, whose definition we do not repeat here. Instead, we note that the function A_3 is totally symmetric under the interchange of its arguments while A_2 is symmetric only in its first two arguments,

$$A_2(p_1, p_2, p_3) = A_2(p_2, p_1, p_3). \quad (33)$$

The amplitude-squared for this contribution, summed over colors and spins, is then given by,

$$\begin{aligned} \mathcal{S}_{ggg} &\equiv -\mathcal{M}_3^{(a),\alpha\beta\gamma\rho\sigma} \left(\mathcal{M}_{3,\alpha\beta\gamma\rho'\sigma'}^{(a)} \right)^* P_{Z\rho'}^{\rho'}(k_4) P_{Z\sigma}^{\sigma'}(k_5) \\ &= |\mathcal{N}|^2 g_s^2 \frac{64VN}{s_{12}s_{23}s_{31}} \frac{s_H^4}{(s_H - M_H^2)^2} \left[8 + \left(\frac{s_H - 2m_Z^2}{m_Z^2} \right)^2 \right] \\ &\times \left[|A_2(p_1, p_2, p_3)|^2 + |A_2(p_2, p_3, p_1)|^2 + |A_2(p_3, p_1, p_2)|^2 + |A_4(p_1, p_2, p_3)|^2 \right]. \end{aligned} \quad (34)$$

The negative sign in the first line comes from the sum over the polarizations of the three gluons. We have introduced a new function A_4 that is defined by,

$$A_4(p_1, p_2, p_3) = [A_2(p_1, p_2, p_3) + A_2(p_2, p_3, p_1) + A_2(p_3, p_1, p_2) - 2A_3(p_1, p_2, p_3)]. \quad (35)$$

As a cross-check, we can inspect the limit $m_q \rightarrow \infty$ in which these functions take the limiting values,

$$A_4(p_1, p_2, p_3) = -\frac{1}{3}; \quad A_2(p_1, p_2, p_3) = -\frac{4p_1 \cdot p_2^2}{3s_H^2}. \quad (36)$$

Thus in this limit the squared amplitude becomes,

$$\mathcal{S}_{ggg} = |\mathcal{N}|^2 g_s^2 \frac{64VN}{9} \frac{1}{(s_H - M_H^2)^2} \left(8 + \left(\frac{s_H - 2m_Z^2}{m_Z^2} \right)^2 \right) \left(\frac{s_H^4 + s_{12}^4 + s_{23}^4 + s_{31}^4}{s_{12}s_{23}s_{31}} \right), \quad (37)$$

which is the expected result [31].

3.5. Projection of interference for $gg \rightarrow ZZg$

Finally, we turn to the background amplitude of process (6). The relevant topologies of diagrams are shown in Fig. 3(c,d). There are 42 diagrams in all, 24 of the topology of Fig. 3(c) and 18 of the topology of Fig. 3(d). The continuum amplitude can be written as,

$$\mathcal{B}_3^{(a),\alpha\beta\gamma\rho\sigma} = -2ig_s\mathcal{N} \left[\text{Tr} (T^A T^B T^C) B_3^{(a),\alpha\beta\gamma\rho\sigma}(1, 2, 3) + \text{Tr} (T^A T^C T^B) B_3^{(a),\alpha\gamma\beta\rho\sigma}(1, 3, 2) \right] \quad (38)$$

where $B_3^{(a),\alpha\beta\gamma\rho\sigma}(1, 2, 3)$ and $B_3^{(a),\alpha\gamma\beta\rho\sigma}(1, 3, 2)$ are color-ordered gauge-invariant primitive amplitudes. Since we are only interested in the interference between $\mathcal{B}_3^{(a)}$ and the Higgs amplitude $\mathcal{M}_3^{(a)}$, and since $\mathcal{M}_3^{(a)}$ is proportional to the antisymmetric color structure f^{ABC} (cf. Eq. (31)), terms proportional to the symmetric color combination d^{ABC} will vanish in the interference and can be safely dropped. Thus the amplitude can be replaced by,

$$\mathcal{B}_3^{(a),\alpha\beta\gamma\rho\sigma} = \frac{1}{2}g_s\mathcal{N}f^{ABC} \left[B_3^{(a),\alpha\beta\gamma\rho\sigma}(1, 2, 3) - B_3^{(a),\beta\alpha\gamma\rho\sigma}(2, 1, 3) \right]. \quad (39)$$

The weak coupling structure of the amplitudes $B_3^{(a)}$ can be written as a linear combination of v_f^2 , a_f^2 and $v_f a_f$, cf. Eq. (15). By inspection of the diagrams it can be seen that, for either purely vector (VV) or purely axial (AA) couplings in the loop, $B_3^{(a),\beta\alpha\gamma\rho\sigma}(2, 1, 3) = -B_3^{(a),\alpha\beta\gamma\rho\sigma}(1, 2, 3)$. In contrast, for the mixed case (VA or AV) the two permutations are equal, $B_3^{(a),\beta\alpha\gamma\rho\sigma}(2, 1, 3) = B_3^{(a),\alpha\beta\gamma\rho\sigma}(1, 2, 3)$. Hence we can simply write,

$$\mathcal{B}_3^{(a),\alpha\beta\gamma\rho\sigma} = g_s\mathcal{N}f^{ABC} B_3^{(a),\alpha\beta\gamma\rho\sigma}(1, 2, 3) \quad (40)$$

and only consider two combinations of vector boson couplings, VV and $AA - VV$.

The interference is given by

$$\mathcal{I}_{ggg} = -2\mathcal{M}_3^{(a),\alpha\beta\gamma\rho'\sigma'} \left(\mathcal{B}_{3,\alpha\beta\gamma\rho\sigma}^{(a)} \right)^* P_{Z\rho'}^\rho(k_4) P_{Z\sigma'}^\sigma(k_5), \quad (41)$$

where again the minus sign comes from the sum over the gluon polarizations. Our strategy will be to contract the continuum amplitudes with the tensors F_1 and F_2 present in the Higgs amplitude, Eq. (31). The definitions of the tensors is given in Eq. (32). Writing this explicitly, we have

$$\mathcal{I}_{ggg} = 8|\mathcal{N}|^2 g_s^2 V N \frac{s_H^2}{(s_H - M_H^2)} P_{Z\rho'}^\rho(k_4) P_Z^{\rho'\sigma}(k_5) \left[\left(A_3(1, 2, 3) F_2^{\alpha\beta\gamma}(1, 2, 3) + \sum_{\tilde{P}(1,2,3)} A_2(1, 2, 3) F_1^{\alpha\beta\gamma}(1, 2, 3) \right) \left(B_{3,\alpha\beta\gamma\rho\sigma}^{(a)}(1, 2, 3) \right)^* \right] \quad (42)$$

where the sum is over the three cyclic permutations. Since $B_3^{(a)}$ is fully symmetric under such permutations, we can write the above as

$$\mathcal{I}_{ggg} = 8|\mathcal{N}|^2 g_s^2 V N \frac{s_H^2}{(s_H - M_H^2)} \left[A_3(1, 2, 3) H_3(1, 2, 3) + \sum_{\tilde{P}(1,2,3)} A_2(1, 2, 3) H_2(1, 2, 3) \right] \quad (43)$$

where

$$\begin{aligned} H_3(1, 2, 3) &= F_2^{\alpha\beta\gamma}(1, 2, 3) \left(B_{3,\alpha\beta\gamma\rho\sigma}^{(a)}(1, 2, 3) \right)^* P_{Z\rho'}^\rho(k_4) P_Z^{\rho'\sigma}(k_5) \\ H_2(1, 2, 3) &= F_1^{\alpha\beta\gamma}(1, 2, 3) \left(B_{3,\alpha\beta\gamma\rho\sigma}^{(a)}(1, 2, 3) \right)^* P_{Z\rho'}^\rho(k_4) P_Z^{\rho'\sigma}(k_5). \end{aligned} \quad (44)$$

In our implementation we have analytically computed $H_3(1, 2, 3)$ and $H_2(1, 2, 3)$ and then performed the sum over the three permutations numerically.

$m_H = 126 \text{ GeV}$	$\Gamma_H = 4.307 \text{ MeV}$	$m_Z = 91.1876 \text{ GeV}$
$m_t = 173.225 \text{ GeV}$	$m_b = 4.75 \text{ GeV}$	$\sin^2 \theta_W = 0.2226459$
$G_F = 1.16639 \times 10^{-5} \text{ GeV}^{-2}$	$g_W^2 = 0.4264904$	$e^2 = 0.0949563$

TABLE IV: Masses, widths and electroweak coupling parameters used in this work.

4. RESULTS

The Higgs and interference amplitudes presented in Secs. 2 and 3 have been implemented in the parton level integrator MCFM, using a library of scalar integrals [36]. In this section we present results for the LHC running at $\sqrt{s} = 8 \text{ TeV}$ and $\sqrt{s} = 13 \text{ TeV}$. Our parameters are summarized in Table IV. Since we are particularly interested in the behavior of the high mass tail, we make use of a dynamic factorization/renormalization scale $\mu = m_{ZZ}/2$. We remind the reader that we consider on-shell Z -bosons, and include their decay only through a branching ratio $BR(Z \rightarrow e^+e^-) = 3.36386 \times 10^{-2}$. Thus, we are insensitive to the details of the lepton kinematics. We demand the presence of a single jet, defined using the anti- k_T algorithm and having a rapidity $|\eta_j| < 3$ and a transverse momentum $p_{T,j} > p_{T,\text{cut}}$. We make use of the MSTW08LO parton distributions functions (pdfs) throughout [37].

We will refer to the cross sections that arise from the signal amplitudes $\mathcal{M}_3^{(a)}$ and $\mathcal{M}_3^{(b)}$ as σ_H^{gg} and $\sigma_H^{qg+q\bar{q}}$ respectively, and their sum as σ_H . Similarly, the cross sections arising from the interference of these amplitudes with $\mathcal{B}_3^{(a)}$ and $\mathcal{B}_3^{(b)}$, respectively, are σ_I^{gg} and $\sigma_I^{qg+q\bar{q}}$; their sum is σ_I . The $q\bar{q}$ -initiated contributions in $\sigma_H^{qg+q\bar{q}}$ and $\sigma_I^{qg+q\bar{q}}$ are at the level of less than one per-mille. The cross section arising from the interference of $\mathcal{M}_3^{(b)}$ with the tree-level amplitude $\mathcal{B}_1^{(b)}$ is σ_I^{tree} . Recall that we do not consider the square of background amplitudes such as $\mathcal{B}_3^{(a)}$, as these contribute at NNLO to the continuum background.

In Table V, we show partonic level cross sections in the high mass tail defined by $m_{ZZ} > 300 \text{ GeV}$. Four different values of the jet cut $p_{T,\text{cut}}$ are shown at center-of-mass energies $\sqrt{s} = 8 \text{ TeV}$ and $\sqrt{s} = 13 \text{ TeV}$. We have confirmed that our results for σ_H^{gg} and σ_I^{gg} agree with those shown in Ref. [22]. Comparing these gg -initiated cross sections with the $qg + q\bar{q}$ -initiated cross sections (which are not considered in Ref. [22]), we see that the former are always larger but the latter are still important, especially at larger values of $p_{T,\text{cut}}$. The relative partonic contributions at a given $p_{T,\text{cut}}$ are roughly the same for Higgs and interference cross sections: at $\sqrt{s} = 8 \text{ TeV}$, both $\sigma_H^{qg+q\bar{q}}/\sigma_H$ and $\sigma_I^{qg+q\bar{q}}/\sigma_I$ are approximately 25% at $p_{T,\text{cut}} = 30 \text{ GeV}$ and increase to almost 50% at $p_{T,\text{cut}} = 200 \text{ GeV}$. This effect is due to the larger $p_{T,\text{cut}}$ probing a higher region of x , where the quark pdfs are relatively more important than the gluon pdfs. At $\sqrt{s} = 13 \text{ TeV}$, the value of x decreases, leading to smaller values for these ratios for a given $p_{T,\text{cut}}$.

The negative values of the interference cross sections are required to restore unitarity. These cross sections are slightly larger in magnitude than the signal rate, so that their sum is negative. The ratio of Higgs to interference is roughly constant for different values of \sqrt{s} or $p_{T,\text{cut}}$, and in either partonic channel. In contrast, the tree-level interference σ_I^{tree} is positive but fairly small, although its importance increases with $p_{T,\text{cut}}$, for the reasons discussed above.

In Table VI we show σ_H and σ_I for the four values of $p_{T,\text{cut}}$ and the two center-of-mass energies. Also shown are the Higgs boson on-peak cross sections (σ_H), defined by $m_{ZZ} < 130 \text{ GeV}$. The latter are obtained by a separate calculation in which the Z -bosons are allowed to be off-shell. The cross sections at $\sqrt{s} = 13 \text{ TeV}$ are a factor of 4–5 times larger than at $\sqrt{s} = 8 \text{ TeV}$, with greater increases coming from higher values of $p_{T,\text{cut}}$. These values indicate that a few events have already been produced in the high mass tail of the one-jet exclusive bin during run I, and about 100 high

	$p_{T,\text{cut}}$ [GeV]	σ_H^{gg} [fb]	σ_H^{gg+qq} [fb]	σ_I^{gg} [fb]	σ_I^{gg+qq} [fb]	σ_I^{tree} [fb]
$\sqrt{s} = 8$ TeV	30	0.0212	0.00679	-0.0299	-0.00929	0.00230
	50	0.0124	0.00522	-0.0173	-0.00706	0.00182
	100	0.00467	0.00279	-0.00632	-0.00369	0.00097
	200	0.00104	0.00086	-0.00133	-0.00111	0.00026
$\sqrt{s} = 13$ TeV	30	0.0887	0.0216	-0.1263	-0.0298	0.00652
	50	0.0547	0.0172	-0.0770	-0.0235	0.00528
	100	0.0229	0.0101	-0.0313	-0.0136	0.00298
	200	0.00612	0.00377	-0.00798	-0.00497	0.00092

TABLE V: Higgs and interference cross sections σ_H and σ_I by partonic channel, for four choices of $p_{T,\text{cut}}$, at the $\sqrt{s} = 8$ TeV and $\sqrt{s} = 13$ TeV LHC. All results shown are in the tail region $m_{ZZ} > 300$ GeV.

	$p_{T,\text{cut}}$ [GeV]	$\sigma_{H,\text{peak}}$ [fb]	$\sigma_{H,\text{tail}}$ [fb]	$\sigma_{I,\text{tail}}$ [fb]	$\sigma_{I,\text{tail}}^{\text{tree}}$ [fb]
$\sqrt{s} = 8$ TeV	30	0.351	0.0280	-0.0392	0.0023
	50	0.206	0.0176	-0.0244	0.0018
	100	0.0714	0.0075	-0.0100	0.0010
	200	0.0128	0.0019	-0.0024	0.00026
$\sqrt{s} = 13$ TeV	30	0.909	0.110	-0.156	0.0065
	50	0.557	0.0718	-0.100	0.0053
	100	0.212	0.0329	-0.0448	0.0030
	200	0.045	0.0099	-0.0130	0.0009

TABLE VI: cross sections at $\sqrt{s} = 8$ and $\sqrt{s} = 13$ TeV in the peak region ($m_{ZZ} < 130$ GeV) and in the high mass tail region defined by $m_{ZZ} > 300$ GeV, for σ_H and σ_I . Also shown is the tree-level interference σ_I^{tree} .

mass events are expected with 300 fb^{-1} at the higher energy. We note that the high mass tail becomes more important relative to the peak cross section as $p_{T,\text{cut}}$ increases because the on-peak cross section is more concentrated at small transverse momentum.

As mentioned in the discussion of Table V, the sum of σ_H and σ_I is negative, and the ratio $|\sigma_I/\sigma_H|$ does not depend appreciably on $p_{T,\text{cut}}$ or \sqrt{s} . The value of σ_I^{tree} is about 5% of the value of σ_I with $p_{T,\text{cut}} = 30$ GeV, and around 10% with $p_{T,\text{cut}} = 200$ GeV. However this contribution will be partially cancelled by the unitarizing effect of the interference between the tree-level amplitudes in process (2) and the one-loop box qg process (3), which is neglected in this paper. We therefore expect the values of $\sigma_{I,\text{tail}}^{\text{tree}}$ given in Table VI to provide an upper bound on the size of the subleading contribution resulting from interference effects involving the tree-level processes.

The dependence of these quantities on the invariant mass of the Z -pair m_{ZZ} is shown in Fig. 6 for $p_{T,\text{cut}} = 30$ GeV and $\sqrt{s} = 8$ TeV. We see that the inclusion of the interference term changes the sign of the Higgs-mediated contribution and its magnitude is significantly reduced, as anticipated. Moreover, the effect of the interference is to dramatically alter the shape of the distribution throughout. This emphasizes the importance of including the interference effects when considering the high mass tail.

As of yet, no mass distributions are available in the one-jet bin, so an extraction of a bound on the Higgs width using our results is not possible. As data become available from the higher energy LHC run, this analysis will become possible. We expect that such a bound will be competitive with the bound extracted from the zero-jet bin. To see this, we can examine the cross section for Higgs-mediated events in the high mass region. We assume that the on-shell Higgs cross-section corresponds to its SM value. This introduces a relationship between the couplings and the Higgs

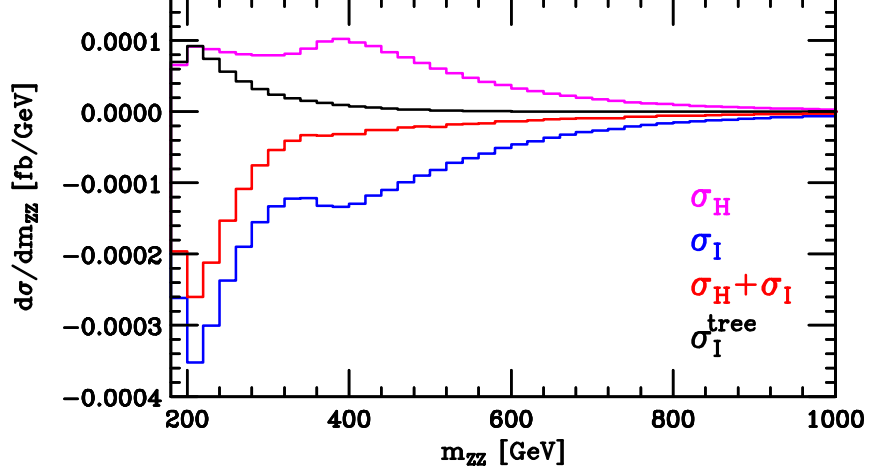


FIG. 6: Higgs and interference distributions σ_H and σ_I , and their sum, for the invariant mass of the Z -pair, m_{ZZ} . Also shown are the tree-level interference distributions σ_I^{tree} . The results were obtained using $p_{T,\text{cut}} = 30$ GeV and $\sqrt{s} = 8$ TeV.

width, which can be used to write the high mass cross-section in terms of the width [4, 5]

$$\sigma_{off,ZZ+jet}^{H+I}(m_{ZZ} > 300 \text{ GeV}) = \sigma_H(m_{ZZ} > 300 \text{ GeV}) \left(\frac{\Gamma_H}{\Gamma_H^{\text{SM}}} \right) + \sigma_I(m_{ZZ} > 300 \text{ GeV}) \sqrt{\frac{\Gamma_H}{\Gamma_H^{\text{SM}}}}. \quad (45)$$

The result for the 4-lepton final state presented in Ref. [4] was,

$$\sigma_{off,4\ell\text{-fiducial}}^{H+I}(m_{4\ell} > 300 \text{ GeV}) = 0.025 \left(\frac{\Gamma_H}{\Gamma_H^{\text{SM}}} \right) - 0.036 \sqrt{\frac{\Gamma_H}{\Gamma_H^{\text{SM}}}} \text{ fb}, \quad (46)$$

where the Z -bosons were produced off-shell, and fiducial cuts were applied to the leptons originating from their decay. In order to compare with the methodology of this paper, we repeat the calculation of Ref. [4] but keep the Z -bosons on-shell and simply apply the appropriate branching ratio into leptons. In this case the result is,

$$\sigma_{off,ZZ}^{H+I}(m_{ZZ} > 300 \text{ GeV}) = 0.0323 \left(\frac{\Gamma_H}{\Gamma_H^{\text{SM}}} \right) - 0.0468 \sqrt{\frac{\Gamma_H}{\Gamma_H^{\text{SM}}}} \text{ fb}. \quad (47)$$

The relative size of the two coefficients in Eqs. (46) and (47) is the same, as might be expected. In the presence of an additional jet, defined with a p_T cut of 30 GeV, the equivalent result is:

$$\sigma_{off,ZZ+jet}^{H+I}(m_{ZZ} > 300 \text{ GeV}) = 0.0280 \left(\frac{\Gamma_H}{\Gamma_H^{\text{SM}}} \right) - 0.0392 \sqrt{\frac{\Gamma_H}{\Gamma_H^{\text{SM}}}} \text{ fb}, \quad (48)$$

where the coefficients have been read from Table VI. Thus the prediction for the effect of the Standard Model Higgs boson on the number of off-shell ZZ +jet events is slightly smaller than the effect on the number of off-shell ZZ events, inclusive in the number of jets. However the scaling with a non-SM value of the width is about the same. The equivalent formulae for other values of the jet cut can be read off from Table VI. We anticipate a more detailed study once further experimental data on ZZ production in the one-jet bin are available.

5. CONCLUSIONS

We have studied the high mass tail of a Higgs boson produced in association with one jet, focusing on the Higgs decay to a Z -boson pair. We have performed the calculation in a simple kinematic configuration with on-shell Z -bosons which are summed over polarizations. The overall Higgs rate in the one-jet bin is known to be large, and we find a significant contribution from the high mass tail for a typical jet transverse momentum and rapidity. This feature has already been noted in the inclusive case, where it has been used to extract a tight bound on the Higgs width. In addition, the ratio of the Higgs signal to the dominant leading order background $pp \rightarrow ZZ + n$ jets is larger in the one-jet bin than in the zero-jet bin. It is therefore desirable to study the high mass tail in the one-jet bin, both in current and future LHC data.

An accurate prediction of the high mass tail requires an understanding of the interference between Higgs-mediated and non-Higgs mediated amplitudes, and we have studied this interference from both the gg and qq production modes. Qualitatively, the effects of the interference are similar to those found in the inclusive case: the interference provides a negative contribution to the high mass tail which is larger in magnitude than the signal rate, leading to a negative shift in the distributions. The interference between the Higgs-mediated one-loop diagrams and tree-level background diagrams is found to be subdominant, despite these entering at a lower order in g_s . A brief analysis shows that the bounds on the Higgs width that can be extracted in this channel are comparable to those from inclusive production. We also point out that the results presented here form an important step to extending the understanding of the high mass tail in the inclusive case to NLO.

Throughout this paper we have considered Higgs production through gluon fusion and neglected the subdominant production mechanism of weak boson fusion (WBF). This mechanism has a distinctive signature of two very forward jets, with little hadronic activity between them. These signatures dominate the two-jet bin, but will also contribute to the one-jet bin if one of the jets is missed by the detector. A Higgs boson produced through WBF must necessarily exhibit similar high mass tail effects, if the Higgs is to unitarize weak boson scattering. Therefore a corroborating analysis should be possible in the WBF production mode, although it will require a careful event selection in order to isolate the Higgs-related contribution from electroweak production of Z -pairs and jets.

While we have focused on $H \rightarrow ZZ$ exclusively, we expect qualitatively similar effects in $H \rightarrow W^+W^-$ decay. However, this decay channel is experimentally challenging in the presence of a jet, due to the large top-pair background. We also note that Higgs results in the exclusive one-jet bin are known to be sensitive to the logarithms of the transverse momentum veto [38]. Moulton and Stewart recently showed [39] that although these logarithms have a mild impact on the Higgs width measurement in $H \rightarrow ZZ$ decay, where the study is rather inclusive in the number of jets, they can have a large effect in the $H \rightarrow W^+W^-$ channel where jet-binning is crucial to the analysis. The LO study that we present in this work should be taken as a starting point, and higher order corrections should be computed when at all possible.

Acknowledgements

RKE would like to thank the RWTH, Aachen for hospitality during the preparation of this paper and would like to acknowledge useful discussions with Michael Czakon and Sebastian Kirchner. RR is grateful to the CERN Theory Group for their hospitality during the preparation of this paper. This research is supported by the US DOE under contract DE-AC02-07CH11359.

Appendix A: Definition of the scalar integrals

We work in the Bjorken-Drell metric so that $l^2 = l_0^2 - l_1^2 - l_2^2 - l_3^2$. The definition of the integrals is as follows

$$\begin{aligned}
B_0(p_1; m_1, m_2) &= \frac{\mu^{4-D}}{i\pi^{\frac{D}{2}} r_\Gamma} \int d^D l \frac{1}{(l^2 - m_1^2 + i\varepsilon)((l + p_1)^2 - m_2^2 + i\varepsilon)}, \\
C_0(p_1, p_2; m_1, m_2, m_3) &= \frac{1}{i\pi^2} \\
&\times \int d^4 l \frac{1}{(l^2 - m_1^2 + i\varepsilon)((l + p_1)^2 - m_2^2 + i\varepsilon)((l + p_1 + p_2)^2 - m_3^2 + i\varepsilon)}, \\
D_0(p_1, p_2, p_3; m_1, m_2, m_3, m_4) &= \frac{1}{i\pi^2} \\
&\times \int d^4 l \frac{1}{(l^2 - m_1^2 + i\varepsilon)((l + p_1)^2 - m_2^2 + i\varepsilon)((l + p_1 + p_2)^2 - m_3^2 + i\varepsilon)((l + p_1 + p_2 + p_3)^2 - m_4^2 + i\varepsilon)},
\end{aligned} \tag{A1}$$

We have removed the overall constant which occurs in D -dimensional integrals

$$r_\Gamma \equiv \frac{\Gamma^2(1 - \epsilon)\Gamma(1 + \epsilon)}{\Gamma(1 - 2\epsilon)} = \frac{1}{\Gamma(1 - \epsilon)} + \mathcal{O}(\epsilon^3) = 1 - \epsilon\gamma + \epsilon^2 \left[\frac{\gamma^2}{2} - \frac{\pi^2}{12} \right] + \mathcal{O}(\epsilon^3). \tag{A2}$$

-
- [1] G. Aad et al. (ATLAS Collaboration), Phys.Lett. **B716**, 1 (2012), 1207.7214.
 - [2] S. Chatrchyan et al. (CMS Collaboration), Phys.Lett. **B716**, 30 (2012), 1207.7235.
 - [3] N. Kauer and G. Passarino, JHEP **1208**, 116 (2012), 1206.4803.
 - [4] J. M. Campbell, R. K. Ellis, and C. Williams, JHEP **1404**, 060 (2014), 1311.3589.
 - [5] F. Caola and K. Melnikov, Phys.Rev. **D88**, 054024 (2013), 1307.4935.
 - [6] J. M. Campbell, R. K. Ellis, and C. Williams, Phys.Rev. **D89**, 053011 (2014), 1312.1628.
 - [7] G. Cacciapaglia, A. Deandrea, G. D. La Rochelle, and J.-B. Flament (2014), 1406.1757.
 - [8] A. Azatov, C. Grojean, A. Paul, and E. Salvioni (2014), 1406.6338.
 - [9] Tech. Rep. ATLAS-CONF-2014-042, CERN, Geneva (2014).
 - [10] V. Khachatryan et al. (CMS Collaboration), Phys.Lett. **B736**, 64 (2014), 1405.3455.
 - [11] C. Englert and M. Spannowsky (2014), 1405.0285.
 - [12] R. K. Ellis, I. Hinchliffe, M. Soldate, and J. van der Bij, Nucl.Phys. **B297**, 221 (1988).
 - [13] Tech. Rep. ATLAS-CONF-2013-072, ATLAS-COM-CONF-2013-086, CERN, Geneva (2013).
 - [14] C. R. Schmidt, Phys.Lett. **B413**, 391 (1997), hep-ph/9707448.
 - [15] D. de Florian, M. Grazzini, and Z. Kunszt, Phys.Rev.Lett. **82**, 5209 (1999), hep-ph/9902483.
 - [16] V. Ravindran, J. Smith, and W. Van Neerven, Nucl.Phys. **B634**, 247 (2002), hep-ph/0201114.
 - [17] C. J. Glosser and C. R. Schmidt, JHEP **0212**, 016 (2002), hep-ph/0209248.
 - [18] R. Boughezal, F. Caola, K. Melnikov, F. Petriello, and M. Schulze, JHEP **1306**, 072 (2013), 1302.6216.
 - [19] X. Chen, T. Gehrmann, E. Glover, and M. Jaquier (2014), 1408.5325.
 - [20] E. N. Glover and J. van der Bij, Nucl.Phys. **B321**, 561 (1989).
 - [21] J. M. Campbell, R. K. Ellis, and C. Williams, JHEP **1110**, 005 (2011), 1107.5569.
 - [22] F. Campanario, Q. Li, M. Rauch, and M. Spira, JHEP **1306**, 069 (2013), 1211.5429.
 - [23] J. M. Campbell, R. K. Ellis, and C. Williams, JHEP **1107**, 018 (2011), 1105.0020.
 - [24] T. Binoth, T. Gleisberg, S. Karg, N. Kauer, and G. Sanguinetti, Phys.Lett. **B683**, 154 (2010), 0911.3181.
 - [25] J. Alwall, R. Frederix, S. Frixione, V. Hirschi, F. Maltoni, et al., JHEP **1407**, 079 (2014), 1405.0301.
 - [26] S. Karg, T. Binoth, T. Gleisberg, N. Kauer, M. Kramer, et al. (2010), 1001.2537.
 - [27] F. Cascioli, T. Gehrmann, M. Grazzini, S. Kallweit, P. Maierhöfer, et al. (2014), 1405.2219.

- [28] F. Cascioli, S. Hoeche, F. Krauss, P. Maierhöfer, S. Pozzorini, et al., JHEP **1401**, 046 (2014), 1309.0500.
- [29] P. Agrawal and A. Shivaaji, Phys.Rev. **D86**, 073013 (2012), 1207.2927.
- [30] T. Melia, K. Melnikov, R. Röntsch, M. Schulze, and G. Zanderighi, JHEP **1208**, 115 (2012), 1205.6987.
- [31] S. Dawson, Nucl.Phys. **B359**, 283 (1991).
- [32] A. Djouadi, M. Spira, and P. Zerwas, Phys.Lett. **B264**, 440 (1991).
- [33] R. K. Ellis, W. J. Stirling, and B. Webber, Camb.Monogr.Part.Phys.Nucl.Phys.Cosmol. **8**, 1 (1996).
- [34] H. Georgi, S. Glashow, M. Machacek, and D. V. Nanopoulos, Phys.Rev.Lett. **40**, 692 (1978).
- [35] G. Passarino and M. J. G. Veltman, Nucl. Phys. **B160**, 151 (1979).
- [36] A. van Hameren, Comput.Phys.Commun. **182**, 2427 (2011), 1007.4716.
- [37] A. Martin, W. Stirling, R. Thorne, and G. Watt, Eur.Phys.J. **C63**, 189 (2009), 0901.0002.
- [38] I. W. Stewart and F. J. Tackmann, Phys.Rev. **D85**, 034011 (2012), 1107.2117.
- [39] I. Moult and I. W. Stewart (2014), 1405.5534.